



Research paper

Efficient photoelectrochemical conversion of CO₂ to syngas by photocathode engineering

Sheng Chu ^{a,b,*},¹ Pengfei Ou ^{c,1}, Roksana Tonny Rashid ^{b,1}, Yuyang Pan ^a, Daolun Liang ^a, Huiyan Zhang ^a, Jun Song ^{c,*}

^a Key Laboratory of Energy Thermal Conversion and Control of Ministry of Education, School of Energy and Environment, Southeast University, Nanjing, 210096, China

^b Department of Electrical and Computer Engineering, McGill University, Montreal, QC H3A 0E9, Canada

^c Department of Mining and Materials Engineering, McGill University, Montreal, QC H3A 0C5, Canada

Received 16 August 2020; revised 20 October 2020; accepted 18 November 2020

Available online 21 November 2020

Abstract

The synthesis of renewable chemical fuels from CO₂ and H₂O via photoelectrochemical (PEC) route represents a promising room-temperature approach for transforming greenhouse gas into value-added chemicals (e.g., syngas), but to date it has been hampered by the lack of efficient photocathode for CO₂ reduction. Herein, we report efficient PEC CO₂ reduction into syngas by photocathode engineering. The photocathode is consisting of a planar p-n Si junction for strong light harvesting, GaN nanowires for efficient electron extraction and transfer, and Au/TiO₂ for rapid electrocatalytic syngas production. The photocathode yields a record-high solar energy conversion efficiency of 2.3%. Furthermore, desirable syngas compositions with CO/H₂ ratios such as 1:2 and 1:1 can be produced by simply varying the size of Au nanoparticle. Theoretical calculations reveal that the active sites for CO and H₂ generation are the facet and undercoordinated sites of Au particles, respectively.

© 2020 Institute of Process Engineering, Chinese Academy of Sciences. Publishing services by Elsevier B.V. on behalf of KeAi Communications Co., Ltd. This is an open access article under the CC BY-NC-ND license (<http://creativecommons.org/licenses/by-nc-nd/4.0/>).

Keywords: Photoelectrocatalysis; CO₂ reduction; Syngas; Size effect; GaN nanowires

1. Introduction

Despite CO₂ is a major greenhouse gas that contributes to global warming, it has also been considered as an abundant carbon source. The conversion of CO₂ into chemical fuels or chemical building blocks is an attractive strategy of turning the waste into assets, which may play a vital role in the green transformation of current energy infrastructure and chemical industry. Among various CO₂ conversion technologies, photoelectrochemical (PEC) approach has been

regarded as a promising route to efficiently reduce CO₂ reduction at mild conditions (e.g., room temperature and ambient pressure), since it takes advantage of synergistic effects of both photo-energy and electricity as energy input for CO₂ reduction [1–13]. The applied external bias facilitates the separation of photogenerated charge carriers, and thus enhances the conversion efficiency. In particular, recently there has been a substantial interest in the conversion of CO₂ into syngas (CO + H₂ mixtures), which is an industrial feedstock for producing synfuels and high-value chemicals [14–22]. To date, various semiconductors including metal oxides [23–26], Si [27–37], GaN [38], ZnTe [39] and perovskite [40] have been exploited as photocathode materials for PEC CO₂ conversion into syngas/CO.

* Corresponding authors.

E-mail address: schu@seu.edu.cn (S. Chu).

¹ S. Chu, P. Ou and R. T. Rashid contributed equally to this work.

Usually, these semiconductor materials are coupled with suitable cocatalysts to accelerate CO₂ conversion and improve the selectivity. Typical electrocatalysts reported for CO₂ reduction to CO include metal particles (e.g., Au, Ag and Zn) [41–44], carbon-based materials [45–47], molecular metal-complexes [48] and single-atom catalysts [49,50]. However, due to the high thermodynamic stability of CO₂ and myriad reaction network to form a variety of products (e.g., CO, HCOOH, CH₄, CH₃OH, HCHO, longer-chain hydrocarbons and alcohols), it remains a challenge to design efficient and selective syngas production from PEC CO₂ reduction. Moreover, the CO/H₂ ratio in the syngas mixture is critical to meet the demands for subsequent downstream thermocatalytic processes [51–61]. For example, methanol synthesis and Fischer–Tropsch hydrocarbon formation requires 1:2 CO/H₂ ratio, whereas in the case of hydroformylation to form aldehyde, CO/H₂ ratio of 1:1 is more desirable. Therefore, developing effective strategies to modulate syngas composition in PEC CO₂ reduction system is equally important for practical applications.

Recently, III-nitride semiconducting materials (e.g., GaN) have received considerable interest for artificial photosynthesis due to their suitable optical properties and band structures [62–66]. The development of molecular beam epitaxy (MBE) technology enables controlled growth of nearly perfect dislocation-free GaN nanowires on wafer-scale planar n⁺-p Si substrate, which emerged as a powerful platform to achieve high-performance optoelectronic and solar conversion devices [67,68]. The GaN/Si platform combines merits of the strong solar absorption of Si (~1.1 eV bandgap) and large charge carrier mobility as well as high-aspect-ratio provided by GaN nanowires. The nanowire arrays minimize the light reflection and therefore enhance the light absorption [69]. In addition, the high exposed surface of nanowire allows high mass loadings of electrocatalyst without compromising light absorption, presenting a powerful and ideal nanoarchitecture for PEC CO₂ conversion. Herein, we report the use of low-dimensional GaN nanowires on planar Si as superior scaffolds to couple with Au/TiO₂ for efficient and tunable PEC syngas production from CO₂ reduction. Experimentally, the photocathode yields a record-high solar-to-syngas efficiency of 2.3%, and enables rational control of syngas mixtures with wide-ranging CO/H₂ ratios by tuning the Au nanoparticle size. Theoretical calculations show that the increase in the proportion of facet sites associated with large Au nanoparticles favors CO₂ reduction to CO over H₂ evolution reaction.

2. Material and methods

2.1. Sample synthesis

The growth of GaN nanowire arrays on a 2-inch planar n⁺-p Si wafer was conducted by a Veeco GEN MBE system without any foreign catalysts [67]. Au particles of 3, 6, 10 and 16 nm were deposited on GaN/n⁺-p Si substrate using a NexDep e-beam evaporator (Angstrom Engineering Inc.) at a deposition rate of 0.01 nm s⁻¹ for 300, 700, 1200 and 2000 s, respectively. Prior to the Au e-beam deposition, the GaN/n⁺-p Si substrate was cleaned with concentrated HCl solution to remove any native oxides. TiO₂ film was deposited on Au/GaN/n⁺-p Si at 225 °C in a Gemstar Arradiance 8 atomic layer deposition (ALD) system, using Tetrakis(dimethylamido)-titanium (TDMAT, Sigma–Aldrich) and deionized water as reactants [70].

2.2. Characterization

This part is shown in the supplementary information.

2.3. PEC measurements

PEC CO₂ reduction was performed in a typical three-electrode cell. Ag/AgCl and Pt wire were adopted as the reference and counter electrode, respectively. The electrolyte was CO₂-saturated 0.5 mol L⁻¹ KHCO₃ (pH 7.5) by purging CO₂ for 30 min. The electrodes were irradiated by a solar simulator (Newport Oriel LCS-100) with a calibrated power intensity of 100 mW cm⁻² at the sample surface. The geometric area of the working electrodes is 0.2–0.3 cm². The PEC data were acquired on an Interface 1000 potentiostat (Gamry Instruments) to measure the current–potential (J–V) curves and chronoamperometry. The gas products after chronoamperometry measurement were quantified by gas chromatograph (GC). H₂ was analyzed by a thermal conductivity detector on Shimadzu GC-8A system, and CO and hydrocarbons were analyzed by a flame ionization detector on Shimadzu GC-2014 system. The possible liquid products were analyzed using NMR spectroscopy (Bruker AV-500). The ¹³C-labeled isotope experiment was performed in ¹³CO₂ (99%, Sigma Aldrich)-saturated ¹³C-bicarbonate solution (NaH¹³CO₃, 98%, Sigma Aldrich). The gas products were analyzed by GC–MS (Agilent 5975).

The half-cell solar-to-syngas efficiency η_{STS} was calculated by the following equation:

$$\eta_{STS}(\%) = \left[\frac{J(\text{mA cm}^{-2}) \times FE_{\text{CO}}(\%) \times (1.34 - V_{\text{bias}})(V) + J(\text{mA cm}^{-2}) \times FE_{\text{H}_2}(\%) \times (1.23 - V_{\text{bias}})(V)}{P_{\text{in}}(\text{mW cm}^{-2})} \right] \quad (1)$$

where J is the recorded photocurrent density of photocathodes, FE_{CO} and FE_{H_2} are faradaic efficiency (FE) for CO and H_2 respectively, V_{bias} is the applied bias versus an ideal counter electrode for O_2 evolution, and P_{in} is power intensity (100 mW cm^{-2}).

2.4. DFT calculations

DFT calculations were conducted with a 400 eV cutoff energy in the Vienna ab initio simulation package (VASP) [71,72] using Bayesian error estimation function with van der Waals correlation [73] and projector augmented wave method [74,75]. The energy convergence and force were set to 10^{-5} eV and 0.01 eV \AA^{-1} , respectively. The four-layer 3×3 (111) and 3×1 (211) surfaces were modeled for the (111) and (211) facets of face-centered cubic metals respectively, both of them contains 9 surface metal atoms with $4 \times 4 \times 1$ Monkhorst-Pack k -point mesh [76]. A vacuum layer of more than 20 \AA in thickness was introduced along the perpendicular direction to separate slabs. The adsorbates and the topmost two layers were allowed for structural relaxation, while the others are fixed to their bulk positions.

The free energy diagrams of H_2 generation and CO_2 reduction reaction were calculated by the model of computational hydrogen electrode (CHE) [77]. As indicated in the previous study [78], the reaction intermediates would be stabilized by the hexagonal water overlayer above them, therefore the solvation correction was also employed by applying a $*COOH$ and $*CO$ stabilization of 0.25 and 0.1 eV, respectively.

3. Results and discussion

3.1. Design and synthesis of photocathode materials

GaN nanowires grown on wafer-scale n^+ -p Si substrate was adopted as the material platform to deposit Au electrocatalyst and construct photocathode for CO_2 reduction into syngas. Au/GaN/ n^+ -p Si sample was prepared using MBE growth of GaN nanowires on n^+ -p Si junction, followed by deposition of Au nanoparticles via e-beam evaporation (Fig. 1a). In the configuration, the optical absorption, charge carrier transportation, and electrocatalytic reaction are spatially and functionally decoupled, providing a powerful platform to rationally investigate the effect of optical, electronic, catalytic modifications on the overall performance. Upon light illumination, the n^+ -p Si with a narrow bandgap of 1.1 eV is readily excited by the major part of sunlight (up to wavelength of 1100 nm) to generate charge carriers. Then the photogenerated electrons from Si can be extracted by the one-dimensional GaN nanowires due to the suitable band alignment between conduction band edges of Si and GaN with heavy n-type doping [67,68]. Finally, the energetic electrons transported through the GaN nanowire to solid/electrolyte interface, for aqueous CO_2 reduction to syngas. The photogenerated holes are conducted to the Si back-contact and transported to the counter anode for water oxidation.

3.2. Structural characterization

SEM characterization of Au/GaN/ n^+ -p Si shows the nanowire array morphology of GaN with a relatively uniform

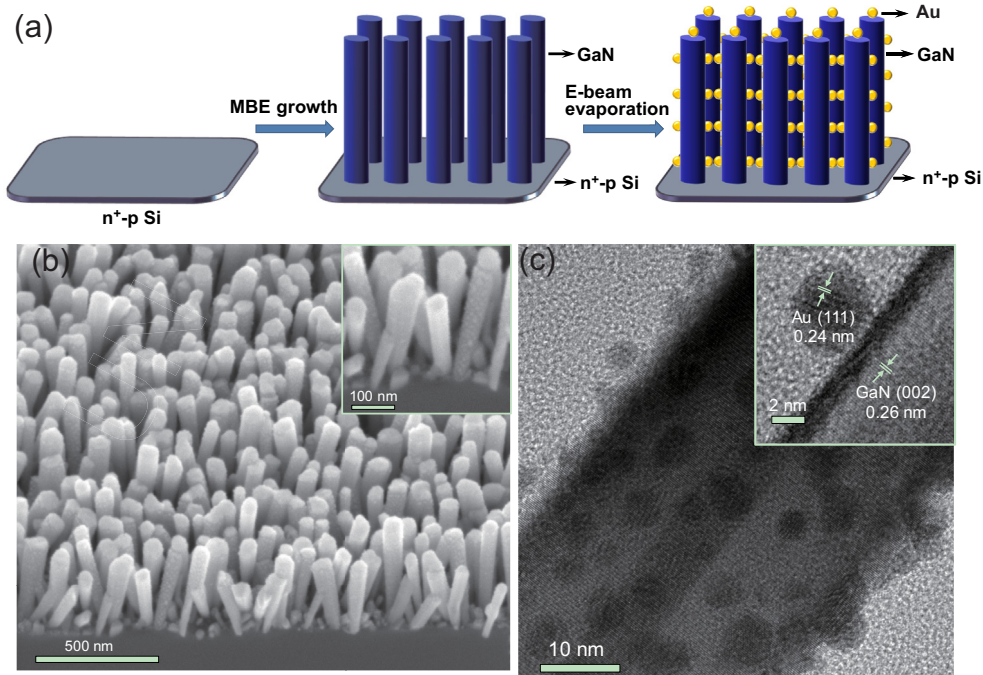


Fig. 1. (a) Schematic illustration for the fabrication of Au/GaN/ n^+ -p Si sample, (b) 45°-tilted SEM, and (c) TEM images of Au nanoparticles on GaN nanowires.

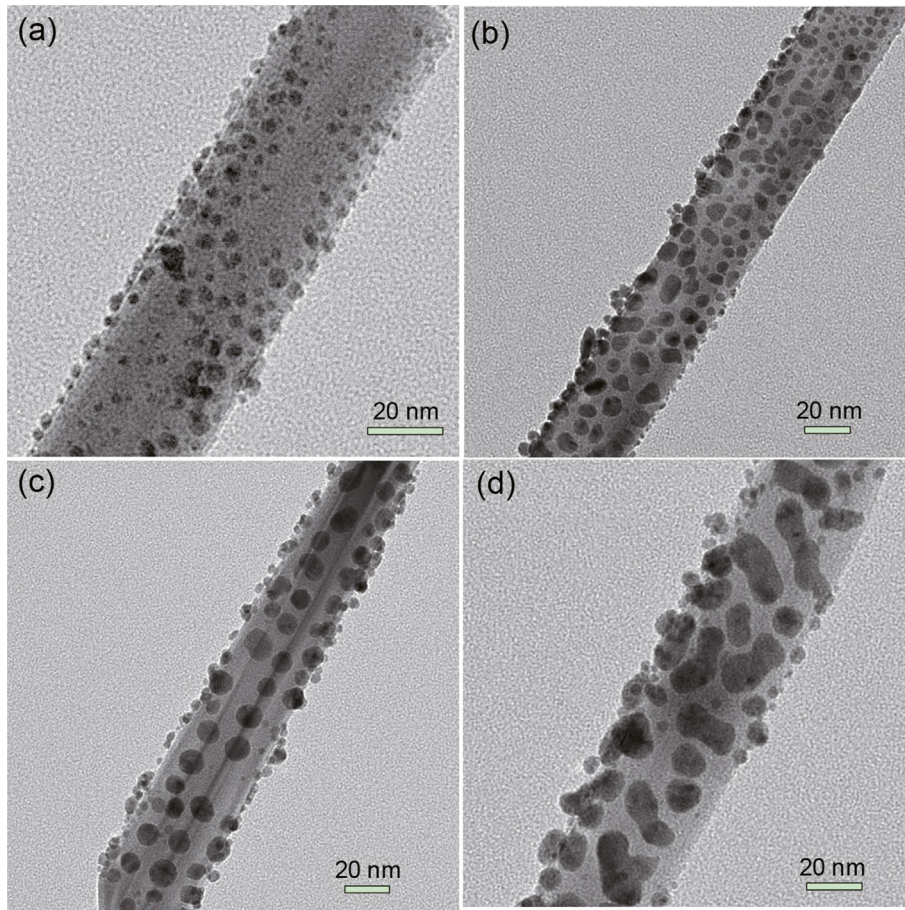


Fig. 2. TEM images of Au nanoparticle with different sizes on GaN nanowires. (a) 3 nm; (b) 6 nm; (c) 10 nm; and (d) 16 nm.

diameter around 40 nm and length of ~350 nm (Fig. 1b). Au nanoparticles with an average size of 6 nm are well distributed across the GaN nanowires (Fig. 1c). High-resolution TEM image in the inset of Fig. 1c shows the (111) facet of Au with a lattice spacing of 0.24 nm. EDX analysis confirms that Au was successfully deposited on GaN nanowires (Fig. S1). And XPS analysis in Fig. S2 indicates metallic Au (Au^0).

Variable-sized Au nanoparticles were obtained by simply varying the e-beam deposition time. TEM images in Fig. 2 show the average diameters of Au nanoparticles to be 3, 6, 10 and 16 nm. The corresponding statistics characteristic of particle size distribution are shown in Fig. S3. The Au nanoparticles with small size are spherical shape, whereas Au nanoparticles with large size are partially coalesced worm-like morphology. XRD analysis were used to evaluate the overall particle sizes of Au nanoparticles. Increasing the size of Au nanoparticles leads to increased intensity of $\text{Au}(111)$ peak, indicating a larger crystalline size of Au nanoparticles (Fig. S4).

3.3. Photoelectrochemical performance

PEC measurements of $\text{Au}/\text{GaN}/\text{n}^+/\text{p}$ Si samples were studied in CO_2 saturated 0.5 mol L^{-1} KHCO_3 aqueous electrolyte (pH 7.5) under one-sun illumination (100 mW cm^{-2} ,

AM 1.5G). Fig. 3a displays the CO and H_2 Faradaic efficiencies (FEs) on photocathodes with different Au sizes at a fixed potential of +0.17 V vs. reversible hydrogen electrode (RHE). It was clearly observed that the product selectivity was largely determined by the Au particle size. An increased selectivity for CO with concurrently decreased selectivity for H_2 was found with the increase in Au particle size. The molar ratio of CO/ H_2 in the products can be adjusted in a large range between 1:11 and 1:1. In particular, 10 nm $\text{Au}/\text{GaN}/\text{n}^+/\text{p}$ Si photoelectrode generated a desirable CO/ H_2 ratio of approximately 1:2, which is suitable for industrial production of methanol and long-chain hydrocarbons via Fischer-Tropsch process [14].

Fig. 3b displays current–potential ($J-V$) plots for $\text{Au}/\text{GaN}/\text{n}^+/\text{p}$ Si photocathodes. All electrodes show negligible currents in the dark. As the size of Au nanoparticle decreases, higher photocurrent density was obtained due to the increase of exposed surface sites. Fig. 3c shows the CO partial current density (J_{CO}) increases and H_2 partial current density decreases with the increase in Au particle size. Increasing the particle size from 3 to 16 nm resulted in an enhancement of J_{CO} by 2.7 times. Fig. 3d shows the FE of CO on $\text{Au}/\text{GaN}/\text{n}^+/\text{p}$ Si photocathodes at various potentials from +0.27 to +0.07 V vs. RHE. The CO FEs are relatively stable in the investigated potential range. Note that different Au loading amounts of the

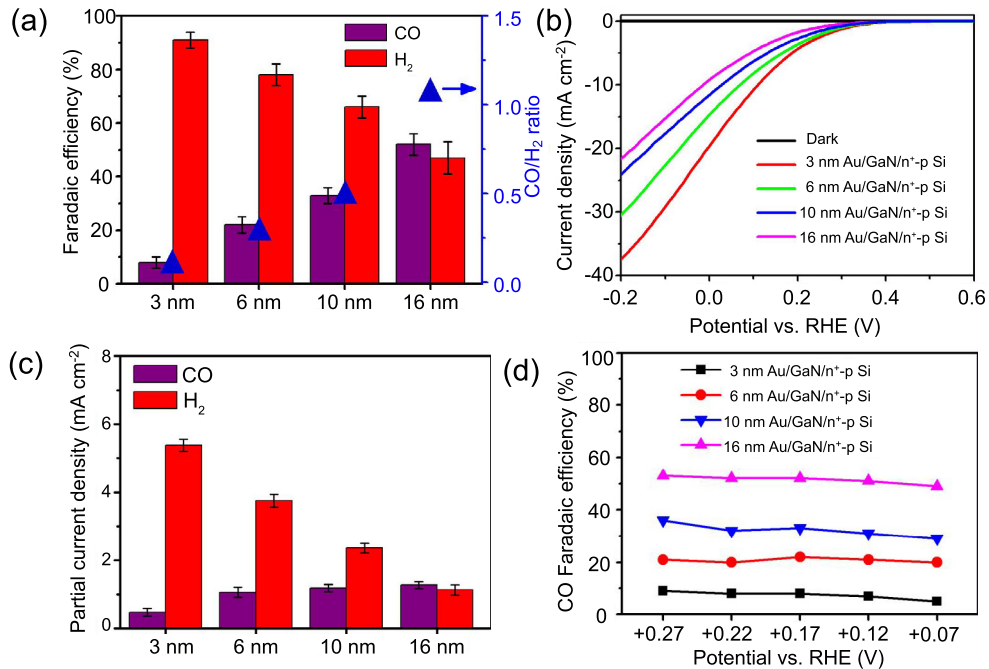


Fig. 3. Size dependence of photoelectrochemical performance on Au nanoparticles. (a) CO and H₂ faradaic efficiencies, and the derived CO/H₂ molar ratios of Au/GaN/n⁺-p Si samples (Experimental conditions: 100 min at +0.17 V vs. RHE). (b) Current–potential curves. (c) Partial current densities. (d) CO faradaic efficiency at different applied potentials.

samples may also affect the catalytic performance, but it is likely that size effect plays a major role in determining the catalytic performance.

3.4. Theoretical studies

To understand the origin of size-dependent syngas composition over Au nanoparticles, theoretical modeling and DFT calculations were performed. It is considered that the reactivity behaviors of metal nanoparticles are determined by

surface sites (i.e., facet, edge and corner) [79–83]. Au nanoparticles were simulated as icosahedron geometry, and the surface site proportion as a function of Au nanoparticle size was plotted in Fig. 4. With the increase of Au nanoparticle size, the proportion of the facet sites increases and the low-coordinated sites (edge and corner) decreases simultaneously. 3 nm Au has a relatively high proportion of low-coordinated sites over 50%, while 16 nm Au is dominated by the facet sites. As a note, the application of different geometries for the simulation of Au nanoparticles will obtain similar qualitative trend. Therefore, the size-dependent CO selectivity can be translated into the different CO and H₂ evolution reactivities over the three different surface sites (i.e., facet, edge and corner).

DFT calculations of the reaction energetics of CO and H₂ evolution reaction were conducted on flat Au(111) surfaces, stepped Au(211) surfaces, and Au13 clusters, which represented the facet, edge and corner, respectively, as shown in Fig. 5. Compared with the facet sites, it was found that CO₂ reduction intermediates *COOH and *CO are stabilized on both the edge and corner sites (Fig. 5a). However, the corner site tends to overbind *CO, which would decrease the desorption rate of CO product and may lead to poisoning of catalyst. In addition, H₂ evolution, the major competitive reaction of aqueous CO₂ reduction, becomes easier from facet, edge to corner, as the energy barrier reduced from 0.60 eV on facet site to 0.43 eV on edge and further to 0.10 eV on corner sites, respectively (Fig. 5b). Therefore, it is inferred that facet sites of Au nanoparticles are active for CO₂ reduction into CO evolution, and the low-coordinated sites are active for H₂ evolution.

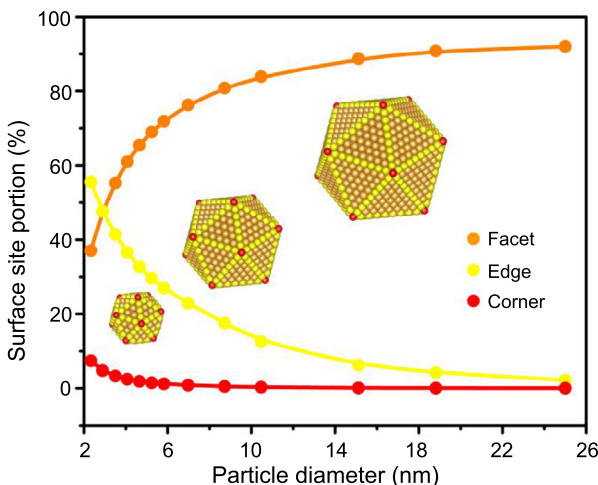


Fig. 4. Portion of surface sites (orange, yellow, and red symbols represent facet, edge and corner, respectively) on icosahedron Au clusters versus Au particle size.

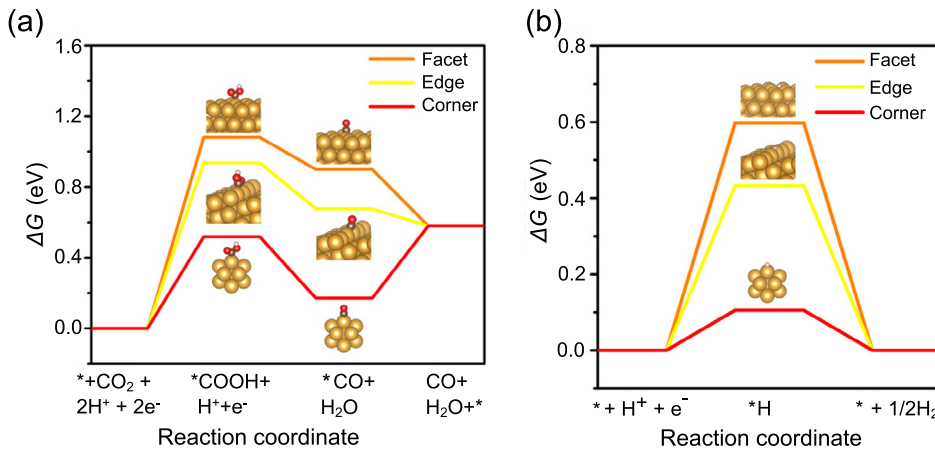


Fig. 5. Free energy diagrams of (a) CO_2 reduction into CO and (b) proton reduction into H_2 on $\text{Au}(111)$ (facet, orange lines), $\text{Au}(211)$ (edge, yellow lines), or Au cluster with 13 atoms (corner, red lines) at 0 V vs. RHE. Au: golden, C: brown, O: red and H: white.

3.5. TiO_2 modification

In terms of PEC performance, the $\text{Au}/\text{GaN}/\text{n}^+/\text{p}$ Si photocathodes were relatively moderate with an onset potential ~ 0.35 V vs. RHE and a photocurrent density of 24 mA cm^{-2} at -0.2 V vs. RHE. However, the performance could be significantly enhanced with a modification of ultrathin TiO_2 overlayer to construct a metal/oxide interface. TiO_2 layer of 0.3 nm thickness was deposited on 10 nm $\text{Au}/\text{GaN}/\text{n}^+/\text{p}$ Si sample using ALD technique, which is a well-established method to

access TiO_2 nanocoating with high conformity at an atomic level [84–86]. XPS analysis confirms the signal of Ti(IV) from TiO_2 (Fig. S5).

Fig. 6a and b show the comparison of J - V curves and FEs for CO , respectively. Compared to bare Au , significantly anodic shift of ~ 100 mV and larger photocurrent were attained with the modification of TiO_2 overlayer. In addition, it is found that the FE towards CO of $\text{Au}-\text{TiO}_2/\text{GaN}/\text{n}^+/\text{p}$ Si exceeds the total amount of that with individual Au or TiO_2 modification (Fig. 6b), indicating a synergy between

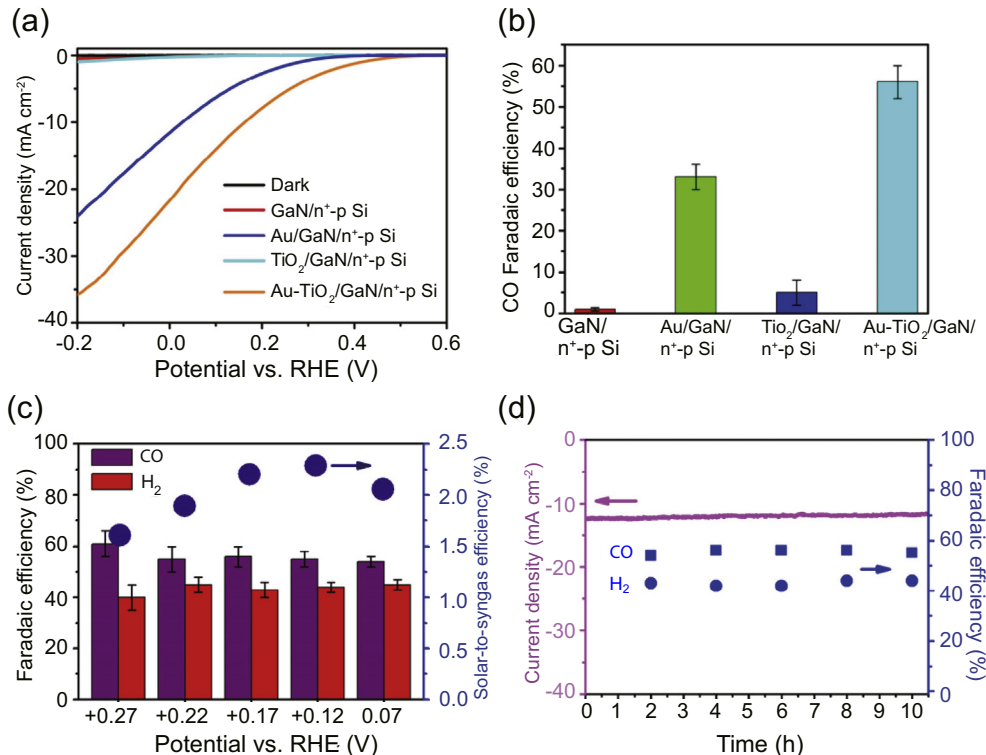


Fig. 6. (a) Current–potential curves. (b) CO faradaic efficiencies at +0.17 V vs. RHE. (c) Faradaic efficiencies towards CO and H_2 , and solar-to-syngas efficiencies of $\text{Au}-\text{TiO}_2/\text{GaN}/\text{n}^+/\text{p}$ Si at different applied potentials. (d) Stability test of $\text{Au}-\text{TiO}_2/\text{GaN}/\text{n}^+/\text{p}$ Si sample at +0.17 V vs. RHE.

Au and TiO₂ for CO evolution from CO₂ reduction. The positive effect of TiO₂ modification on CO generation was also confirmed in other samples with different Au nanoparticle sizes (Fig. S6). It is supposed that the formation of Au/TiO₂ as a metal/oxide interface gives multifunctional and diverse adsorption/reaction sites for CO₂ conversion into syngas [31,87,88]. The CO₂ adsorption–desorption measurements in Fig. S7 show CO₂ adsorption amount is 2.29 μmol cm⁻² over Au–TiO₂/GaN/n⁺-p Si, which is more than four times larger than that on bare Au sample (0.57 μmol cm⁻²). Additionally, the surface trapping states of nanowire may be passivated by the ultrathin TiO₂ overlayer, which suppresses the charge recombination and enhances the PEC efficiency [89,90]. As a control experiment, Au decorated TiO₂/GaN/Si sample was prepared and tested to check the different place effects of Au or TiO₂ in the hybrid. It showed a CO FE of 48%, which was close to that of TiO₂-covered Au/GaN/Si sample (56%). It is likely that ultrathin TiO₂ overlayer of 0.3 nm thickness does not affect the mass transport of reactant and product species associated with syngas generation reaction. However, a negative effect was observed when the thickness of TiO₂ overlayer was more than 1 nm (Fig. S8). The decreased PEC performance with a thick TiO₂ overlayer can be ascribed to its large resistance to inhibit the mass/charge transfer across semiconductor/electrolyte junction [91].

Fig. 6c shows the CO and H₂ FEs over Au–TiO₂/GaN/n⁺-p Si within potential range from +0.27 to +0.07 V vs. RHE. At all potentials investigated, the electrode exhibited a CO FE of 57 ± 4% and H₂ FE of 42 ± 3%. The half-cell solar-to-syngas efficiencies were calculated according to Eq. (1) (see in section of Material and methods and Table S1). As shown in Fig. 6c, at +0.12 V vs. RHE, solar-to-syngas efficiency reached 2.3%, which is higher than that of reported photocathodes [31,33] and sets a new record to our knowledge (see Table S2). Stability testing was also performed, showing no observable degradation and stable products selectivity during 10 h operation (Fig. 6d). The morphology of nanowire arrays and nanoparticle catalysts did not change after the stability test (Fig. S9). The turnover number (TON) for CO was calculated to be ~18,400, considering evolved CO amount of 129 μmol and Au–TiO₂ catalyst of 7 nmol. The catalyst loading amounts were determined by ICP-AES analysis. To identify the carbon source of CO formation, isotope labeling test using ¹³CO₂ was performed. The observation of ¹³CO signal in the GC–MS analysis confirmed the carbon source of CO originated from CO₂ conversion (Fig. S10).

4. Conclusions

Efficient and controllable PEC syngas generation from CO₂ reduction have been demonstrated by coupling Au/TiO₂ catalyst with GaN/n⁺-p Si. The integrated photocathode exhibited a record solar energy conversion efficiency of 2.3%. Moreover, desirable syngas compositions with CO/H₂ ratios such as 1:2 and 1:1 were produced by simply tuning the particle size of Au nanoparticles. The theoretical investigations

revealed that the facet sites of Au particles were active for CO₂ reduction towards CO, and the low-coordinated sites favored the H₂ evolution reaction. This work provides a paradigm to develop efficient PEC CO₂ reduction using rationally designed photoelectrode.

Conflict of interest

The authors declare that they have no known competing financial interests or personal relationships that could have appeared to influence the work reported in this paper.

Acknowledgments

This work was supported by the National Natural Science Foundation of China (22005048, 51822604, 51906040), the Natural Science Foundation of Jiangsu Province (Grants No BK20200399), Emissions Reduction Alberta (ERA), McGill Engineering Doctoral Award, National Sciences and Engineering Research Council (NSERC) Discovery grant (grant # RGPIN-2017-05187). We are also grateful for Supercomputer Consortium Laval UQAM McGill and Eastern Quebec for providing computing power. Sheng Chu would like to thank the support from “Zhishan Young Scholar” Program of Southeast University. Sheng Chu also acknowledges the fruitful discussion with Prof. Z. Mi.

Appendix A. Supplementary data

Supplementary data to this article can be found online at <https://doi.org/10.1016/j.gee.2020.11.015>.

References

- [1] B. Kumar, M. Llorente, J. Froehlich, T. Dang, A. Sathrum, C.P. Kubiak, Annu. Rev. Phys. Chem. 63 (2012) 541–569.
- [2] J.L. White, M.F. Baruch, J.E. Pander, Y. Hu, I.C. Fortmeyer, J.E. Park, T. Zhang, K. Liao, J. Gu, Y. Yan, T.W. Shaw, E. Abelev, A.B. Bocarsly, Chem. Rev. 115 (2015) 12888–12935.
- [3] S.J. Xie, Q.H. Zhang, G.D. Liu, Y. Wang, Chem. Commun. 52 (2016) 35–59.
- [4] L. Zhang, Z.J. Zhao, T. Wang, J.L. Gong, Chem. Soc. Rev. 47 (2018) 5423–5443.
- [5] P.L. Wang, S.C. Wang, H.Q. Wang, Z.B. Wu, L.Z. Wang, Part. Part. Syst. Charact. 35 (2018) 1700371.
- [6] H. Pang, T. Masuda, J.H. Ye, Chem. Asian J. 13 (2018) 127–142.
- [7] E. Kalamaras, M.M. Maroto-Valer, M.H. Shao, J. Xuan, H.Z. Wang, Catal. Today 317 (2018) 56–75.
- [8] N. Zhang, R. Long, C. Gao, Y.J. Xiong, Sci. China Mater. 61 (2018) 771–805.
- [9] V. Kumaravel, J. Bartlett, S.C. Pillai, ACS Energy Lett. 5 (2020) 486–519.
- [10] P. Ding, T. Jiang, N. Han, Y. Li, Mater. Today Nano 10 (2020) 100077.
- [11] Y. Liu, L. Guo, J. Chem. Phys. 152 (2020) 100901.
- [12] J.Y. Wang, Y.J. Guan, X.G. Yu, Y.Z. Cao, J.Z. Chen, Y.L. Wang, B. Hu, H.W. Jing, iScience 23 (2020) 100768.
- [13] J.Y. Feng, H.T. Huang, S.C. Yan, W.J. Luo, T. Yu, Z.S. Li, Z.G. Zou, Nano Today 30 (2020) 100830.
- [14] S.R. Foit, I.C. Vinke, L.G.J. de Haart, R.A. Eichel, Angew. Chem. Int. Ed. 56 (2017) 5402–5411.
- [15] P. Furler, J.R. Scheffe, A. Steinfeld, Energy Environ. Sci. 5 (2012) 6098–6103.

- [16] F.F. Li, J. Lau, S. Licht, *Adv. Sci.* 2 (2015) 1500260.
- [17] D.W. Li, S.X. Ouyang, H. Xu, D. Lu, M. Zhao, X.L. Zhang, J.H. Ye, *Chem. Commun.* 52 (2016) 5989–5992.
- [18] F. Urbain, P.Y. Tang, N.M. Carretero, T. Andreu, L.G. Gerling, C. Voz, J. Arbiol, J.R. Morante, *Energy Environ. Sci.* 10 (2017) 2256–2266.
- [19] A. Tavasoli, G. Ozin, *Joule* 2 (2018) 571–575.
- [20] H.W. Zhang, J.T. Ming, J.W. Zhao, Q. Gu, C. Xu, Z.X. Ding, R.S. Yuan, Z.Z. Zhang, H.X. Lin, X.X. Wang, J.L. Long, *Angew. Chem. Int. Ed.* 58 (2019) 7718–7722.
- [21] A. Li, T. Wang, X. Chang, Z.J. Zhao, C. Li, Z. Huang, P. Yang, G. Zhou, J. Gong, *Chem. Sci.* 9 (2018) 5334–5340.
- [22] M. Chen, J. Wu, C. Lu, X. Luo, Y. Huang, B. Jin, H. Gao, X. Zhang, M. Argyle, Z. Liang, *Green Energy Environ.* 6 (2021) 938–951.
- [23] M. Schreier, P. Gao, M.T. Mayer, J.S. Luo, T. Moehl, M.K. Nazeeruddin, S.D. Tilley, M. Gratzel, *Energy Environ. Sci.* 8 (2015) 855–861.
- [24] G. Sahara, R. Abe, M. Higashi, T. Morikawa, K. Maeda, Y. Ueda, O. Ishitani, *Chem. Commun.* 51 (2015) 10722–10725.
- [25] X. Deng, R. Li, S.K. Wu, L. Wang, J.H. Hu, J. Ma, W.B. Jiang, N. Zhang, X.S. Zheng, C. Gao, L.J. Wang, Q. Zhang, J.F. Zhu, Y.J. Xiong, *J. Am. Chem. Soc.* 141 (2019) 10924–10929.
- [26] X.L. Gu, L.P. Qian, G.F. Zheng, *Mol. Catal.* 492 (2020) 110953.
- [27] Q. Kong, D. Kim, C. Liu, Y. Yu, Y.D. Su, Y.F. Li, P.D. Yang, *Nano Lett.* 16 (2016) 5675–5680.
- [28] D. He, T. Jin, W. Li, S. Pantovich, D.W. Wang, G.H. Li, *Chem. Eur. J.* 22 (2016) 13064–13067.
- [29] S. Chu, S.Z. Fan, Y.J. Wang, D. Rossouw, Y.C. Wang, G.A. Botton, Z. Mi, *Angew. Chem. Int. Ed.* 55 (2016) 14260–14264.
- [30] J.T. Song, H. Ryoo, M. Cho, J. Kim, J.G. Kim, S.Y. Chung, J. Oh, *Adv. Energy Mater.* 7 (2017) 1601103.
- [31] S. Chu, P. Ou, P. Ghamari, S. Vanka, B. Zhou, I. Shih, J. Song, Z. Mi, *J. Am. Chem. Soc.* 140 (2018) 7869–7877.
- [32] Y.P. Hu, F.J. Chen, P. Ding, H. Yang, J.M. Chen, C.Y. Zha, Y.G. Li, *J. Mater. Chem. A* 6 (2018) 21906–21912.
- [33] C.C. Li, T. Wang, B. Liu, M.X. Chen, A. Li, G. Zhang, M.Y. Du, H. Wang, S.F. Liu, J.L. Gong, *Energy Environ. Sci.* 12 (2019) 923–928.
- [34] H. Pang, G. Yang, P. Li, H. Huang, F. Ichihara, T. Takei, J. Ye, *Catal. Today* 339 (2019) 321–327.
- [35] L. Wei, J. Lin, S. Xie, W. Ma, Q. Zhang, Z. Shen, Y. Wang, *Nanoscale* 11 (2019) 12530–12536.
- [36] S. Chu, P. Ou, R.T. Rashid, P. Ghamari, R. Wang, H.N. Tran, S. Zhao, H. Zhang, J. Song, Z. Mi, *iScience* 23 (2020) 101390.
- [37] C. Kim, S. Choi, M.J. Choi, S.A. Lee, S.H. Ahn, S.Y. Kim, H.W. Jang, *Appl. Sci.* 10 (2020) 3487.
- [38] J.S. DuChene, G. Tagliabue, A.J. Welch, W.H. Cheng, H.A. Atwater, *Nano Lett.* 18 (2018) 2545–2550.
- [39] J.W. Jang, S. Cho, G. Magesh, Y.J. Jang, J.Y. Kim, W.Y. Kim, J.K. Seo, S. Kim, K.H. Lee, J.S. Lee, *Angew. Chem. Int. Ed.* 53 (2014) 5852–5857.
- [40] V. Andrei, B. Reuillard, E. Reisner, *Nat. Mater.* 19 (2020) 189–194.
- [41] Y.H. Chen, C.W. Li, M.W. Kanan, *J. Am. Chem. Soc.* 134 (2012) 19969–19972.
- [42] M. Liu, Y.J. Pang, B. Zhang, P. de Luna, O. Voznyy, J.X. Xu, X.L. Zheng, C.T. Dinh, F.J. Fan, C.H. Cao, F.P.G. de Arquer, T.S. Safaei, A. Mepham, A. Klinkova, E. Kumacheva, T. Filleter, D. Sinton, S.O. Kelley, E.H. Sargent, *Nature* 537 (2016) 382.
- [43] Q. Lu, J. Rosen, Y. Zhou, G.S. Hutchings, Y.C. Kimmel, J.G.G. Chen, F. Jiao, *Nat. Commun.* 5 (2014) 3242.
- [44] H.S. Jeon, I. Sinev, F. Scholten, N.J. Divins, I. Zegkinoglou, L. Pielsticker, B.R. Cuenya, *J. Am. Chem. Soc.* 140 (2018) 9383–9386.
- [45] A. Vasileff, Y. Zheng, S.Z. Qiao, *Adv. Energy Mater.* 7 (2017) 1700759.
- [46] N.N. Meng, W. Zhou, Y.F. Yu, Y. Liu, B. Zhang, *ACS Catal.* 9 (2019) 10983–10989.
- [47] Y. Ji, Y.M. Shi, C.B. Liu, B. Zhang, *Sci. China Mater.* 63 (2020) 2351–2357.
- [48] H. Takeda, C. Cometto, O. Ishitani, M. Robert, *ACS Catal.* 7 (2017) 70–88.
- [49] K. Jiang, S. Siahrostami, A.J. Akey, Y.B. Li, Z.Y. Lu, J. Lattimer, Y.F. Hu, C. Stokes, M. Gangishetty, G.X. Chen, Y.W. Zhou, W. Hill, W.B. Cai, D. Bell, K.R. Chan, J.K. Norskov, Y. Cui, H.T. Wang, *Inside Chem.* 3 (2017) 950–960.
- [50] J. Gu, C.S. Hsu, L.C. Bai, H.M. Chen, X.L. Hu, *Science* 364 (2019) 1091.
- [51] P. Kang, Z. Chen, A. Nayak, S. Zhang, T.J. Meyer, *Energy Environ. Sci.* 7 (2014) 4007–4012.
- [52] W. Sheng, S. Kattel, S. Yao, B. Yan, Z. Liang, C.J. Hawhurst, Q. Wu, J.G. Chen, *Energy Environ. Sci.* 10 (2017) 1180–1185.
- [53] S.J. Guo, S.Q. Zhao, X.Q. Wu, H. Li, Y.J. Zhou, C. Zhu, N.J. Yang, X. Jiang, J. Gao, L. Bai, Y. Liu, Y. Lifshitz, S.T. Lee, Z.H. Kang, *Nat. Commun.* 8 (2017) 1828.
- [54] S. Hernández, M. Amin Farkhondehfal, F. Sastre, M. Makkee, G. Saracco, N. Russo, *Green Chem.* 19 (2017) 2326–2346.
- [55] R. He, A. Zhang, Y. Ding, T. Kong, Q. Xiao, H. Li, Y. Liu, J. Zeng, *Adv. Mater.* 30 (2018) 1705872.
- [56] M.B. Ross, Y. Li, P. De Luna, D. Kim, E.H. Sargent, P. Yang, *Joule* 3 (2019) 257–264.
- [57] P. Chen, Y. Jiao, Y.-H. Zhu, S.-M. Chen, L. Song, M. Jaroniec, Y. Zheng, S.Z. Qiao, *J. Mater. Chem. A* 7 (2019) 7675–7682.
- [58] H. Li, P. Wen, D.S. Itanze, Z.D. Hood, X. Ma, M. Kim, S. Adhikari, C. Lu, C.C. Dun, M.F. Chi, Y.J. Qiu, S.M. Geyer, *Nat. Commun.* 10 (2019) 5724.
- [59] N.N. Meng, C.B. Liu, Y. Liu, Y.F. Yu, B. Zhang, *Angew. Chem. Int. Ed.* 58 (2019) 18908–18912.
- [60] D.X. Yang, Q.G. Zhu, X.F. Sun, C.J. Chen, W.W. Guo, G.Y. Yang, B.X. Han, *Angew. Chem. Int. Ed.* 59 (2020) 2354–2359.
- [61] X. Wang, Z.L. Wang, Y. Bai, L. Tan, Y.Q. Xu, X.J. Hao, J.K. Wang, A.H. Mahadi, Y.F. Zhao, L.R. Zheng, Y.F. Song, *J. Energy Chem.* 46 (2020) 1–7.
- [62] M.G. Kibria, Z. Mi, *J. Mater. Chem. A* 4 (2016) 2801–2820.
- [63] U. Chatterjee, J.H. Park, D.Y. Um, C.R. Lee, *Renew. Sustain. Energy Rev.* 79 (2017) 1002–1015.
- [64] S. Chu, X. Kong, S. Vanka, H. Guo, Z. Mi, *Semiconduct. Semimet.* 97 (2017) 223–255.
- [65] P. Varadhan, H.C. Fu, D. Priante, J.R.D. Retamal, C. Zhao, M. Ebaid, T.K. Ng, I. Ajia, S. Mitra, I.S. Roqan, B.S. Ooi, J.H. He, *Nano Lett.* 17 (2017) 1520–1528.
- [66] X. Liu, F.A. Chowdhury, S. Vanka, S. Chu, Z. Mi, *Phys. Status Solidi* 217 (2020) 1900885.
- [67] S. Vanka, E. Arcia, S. Cheng, K. Sun, G.A. Botton, G. Teeter, Z. Mi, *Nano Lett.* 18 (2018) 6530–6537.
- [68] B. Zhou, X. Kong, S. Vanka, S. Chu, P. Ghamari, Y. Wang, N. Pant, I. Shih, H. Guo, Z. Mi, *Nat. Commun.* 9 (2018) 3856.
- [69] J. Deng, Y.D. Su, D. Liu, P.D. Yang, B. Liu, C. Liu, *Chem. Rev.* 119 (2019) 9221–9259.
- [70] S. Chu, S. Vanka, Y. Wang, J. Gim, Y. Wang, Y.-H. Ra, R. Hovden, H. Guo, I. Shih, Z. Mi, *ACS Energy Lett.* 3 (2018) 307–314.
- [71] G. Kresse, J. Hafner, *Phys. Rev. B* 49 (1994) 14251.
- [72] G. Kresse, J. Furthmüller, *Comput. Mater. Sci.* 6 (1996) 15–50.
- [73] J. Wellendorff, K.T. Lundgaard, A. Møgelbøj, V. Petzold, D.D. Landis, J.K. Nørskov, T. Bligaard, K.W. Jacobsen, *Phys. Rev. B* 85 (2012) 235149.
- [74] P.E. Blöchl, *Phys. Rev. B* 50 (1994) 17953.
- [75] G. Kresse, D. Joubert, *Phys. Rev. B* 59 (1999) 1758.
- [76] H.J. Monkhorst, J.D. Pack, *Phys. Rev. B* 13 (1976) 5188.
- [77] J.K. Nørskov, J. Rossmeisl, A. Logadottir, L. Lindqvist, J.R. Kitchin, T. Bligaard, H. Jonsson, *J. Phys. Chem. B* 108 (2004) 17886–17892.
- [78] V. Tripković, E. Skúladóson, S. Siahrostami, J.K. Nørskov, J. Rossmeisl, *Electrochim. Acta* 55 (2010) 7975–7981.
- [79] C. Dong, C. Lian, S. Hu, Z. Deng, J. Gong, M. Li, H. Liu, M. Xing, J. Zhang, *Nat. Commun.* 9 (2018) 1252.
- [80] D. Gao, H. Zhou, J. Wang, S. Miao, F. Yang, G. Wang, J. Wang, X. Bao, *J. Am. Chem. Soc.* 137 (2015) 4288–4291.
- [81] R. Reske, H. Mistry, F. Behafarid, B.R. Cuenya, P. Strasser, *J. Am. Chem. Soc.* 136 (2014) 6978–6986.
- [82] H. Mistry, R. Reske, Z. Zeng, Z.J. Zhao, J. Greeley, P. Strasser, B.R. Cuenya, *J. Am. Chem. Soc.* 136 (2014) 16473–16476.

- [83] W. Zhu, R. Michalsky, O. Metin, H. Lv, S. Guo, C.J. Wright, X. Sun, A.A. Peterson, S. Sun, *J. Am. Chem. Soc.* 135 (2013) 16833–16836.
- [84] T. Wang, Z. Luo, C. Li, J. Gong, *Chem. Soc. Rev.* 43 (2014) 7469–7484.
- [85] R.W. Johnson, A. Hultqvist, S.F. Bent, *Mater. Today* 17 (2014) 236–246.
- [86] A.G. Scheuermann, P.C. McIntyre, *J. Phys. Chem. Lett.* 7 (2016) 2867–2878.
- [87] S. Kattel, P. Liu, J.G. Chen, *J. Am. Chem. Soc.* 139 (2017) 9739–9754.
- [88] D.F. Gao, Y. Zhang, Z.W. Zhou, F. Cai, X.F. Zhao, W.G. Huang, Y.S. Li, J.F. Zhu, P. Liu, F. Yang, G.X. Wang, X.H. Bao, *J. Am. Chem. Soc.* 139 (2017) 5652–5655.
- [89] J. Qiu, G. Zeng, M.A. Ha, M. Ge, Y. Lin, M. Hettick, B. Hou, A.N. Alexandrova, A. Javey, S.B. Cronin, *Nano Lett.* 15 (2015) 6177–6181.
- [90] P. Zhang, T. Wang, J.L. Gong, *Chem. Commun.* 52 (2016) 8806–8809.
- [91] H.J. Kim, K.L. Kearney, L.H. Le, Z.J. Haber, A.A. Rockett, M.J. Rose, *J. Phys. Chem. C* 120 (2016) 25697–25708.